Proceedings of HT-FED2004
USA ASME Heat Transfer/Fluids Engineering Summer Conference
July 11-15, 2004, Charlotte, North Carolina, USA

HT-FED2004-56478

NUMERICAL STUDY OF SWIRLING IMPINGING JETS WITH HEAT TRANSFER

Thomas Hällqvist *
Department of Mechanics
Royal Institute of Technology
S-100 44 Stockholm
Sweden
Email: thom@mech.kth.se

Laszlo Fuchs †
Department of Mechanics
Royal Institute of Technology
S-100 44 Stockholm
Sweden
Email: lf@mech.kth.se

ABSTRACT

This paper deals with numerical simulations of circular impinging jets with heat transfer, by means of Large Eddy Simulation (LES). The LES code uses higher order finite-differences on staggered Cartesian non-uniform grids. The current LES have the potential of dealing with transition as well as providing data on details of larger scale structures, statistical correlations and turbulent spectral content. The impinging circular jet has a nozzle-to-plate spacing ranging from 0.5 *to* 2 *nozzle diameters and the Reynolds number is* 20000*. Three different swirl numbers have been considered, ranging from non-swirling to strongly swirling flow. From the LES results the transition process in the jet is clearly detected. Swirling flow strongly influences the development of the jet. The wall heat transfer rates become obstructed, even though the turbulence level increases.*

INTRODUCTION

With the impinging jet configuration high heat- or mass-transfer rates are efficiently achieved. Therefore, it is widely used in industrial applications. Common application areas are cooling of electrical components and gas turbines combustion chambers. It is also used in processing of metal and glass. Most studies of impinging jets are related to simplified geometries as compared to practical applications. This is so since much of the physics is captured also in the simplest case (flat impingement wall). Effects of particular details of the application (such as swirl, curved impingement walls) may be studied separately and thereby expose the effects of these parameters. The wall heat-transfer rate strongly depends on a number of parameters. For instance the ratio between the characteristic height and diameter of the jet and the character of the incoming jet flow.

There are numerous work done on non-swirling impinging jets. Among others, [1] studied the influence from turbulent separation, induced by strong secondary vortices, on wall heat transfer. Related work were performed by [2], who applied control of vortex formation and also studied the influence on wall heat transfer. Influence from nozzle outlet velocity profiles were studied by [3]. Studies of swirling impinging jets have been conducted by among others, [4]. They studied the influence on wall heat transfer characteristics for different swirl levels. Also [5] performed experimental work on swirling round impinging jets.

Related to the study of swirling impinging jets, is the study of vortex breakdown for free jets. For a free circular swirling jet there are several different modes or states of breakdown. As shown by [6] the first breakdown forms as an axi-symmetric recirculation bubble. The flow then becomes stabilized and then breaks down, a second time, into a helical shape. [7] studied the characteristics of various breakdown states. They identified four distinct forms of vortex breakdown. These include, the above mentioned bubble and helical modes. In non swirling jets the, so called, Kelvin-Helmholtz instability initiates the rolling up of axi-symmetric vortices. In addition, also helical modes may emerge. With swirl, an additional shear-layer instability is present, causing role-up of vortices in the azimuthal direction.

*Address all correspondence to this author.
†Also at Department of Heat and Power Engineering, Lund Institute of Technology.

Two modes can be defined. One due to axial-shear, the axi-symmetric mode ($m = 0$), and the one due to azimuthal shear, the helical mode ($m \neq 0$). For highly swirling flows the $m \neq 0$ modes, azimuthal perturbations, is dominant. In conjunction with the shear instability for swirling flows there may also be contributions from centrifugal instabilities as the azimuthal velocity distribution of the swirling jet satisfies the Rayleigh criterion ([7]).

GOVERNING EQUATIONS

The motion of fluids is fully described by the continuity equation and the Navier Stokes equations. The latter ones are, in dimensionless form, written as

$$\frac{\partial u_i}{\partial t} + \frac{\partial}{\partial x_j}(u_i u_j) = -\frac{\partial p}{\partial x_i} + \frac{1}{Re}\frac{\partial}{\partial x_j}\frac{\partial u_i}{\partial x_j}, \tag{1}$$

where *Re* is the Reynolds number.

With the assumption of temperature being a passive scalar, *i.e.* no influence on the velocity field, the following transport equation can be used to predict heat transfer

$$\frac{\partial c}{\partial t} + u_j\frac{\partial c}{\partial x_j} = \Gamma\frac{\partial}{\partial x_j}\frac{\partial c}{\partial x_j}, \tag{2}$$

where Γ is the diffusivity and c is the concentration of the passive scalar. Here, the diffusive flux of the scalar is assumed to be proportional to the gradient of the scalar. The scalar is referred to as conserved since there is no sink or source term in the transport equation above. As c corresponds to temperature, Γ represents thermal diffusivity, commonly referred to as α, and ν/Γ is the Prandtl number, *Pr*.

TURBULENCE MODELING AND NUMERICS

To fully describe a turbulent flow, all scales of the motion, from the largest energetic scales, ℓ_0, to the smallest Kolmogorov scales, η, must be resolved. The computational requirement for resolving all the scales of the Navier Stokes equations is out of reach for more complex geometries. If one is interested in the dynamics of the flow and/or when the RANS framework is inadequate one may use Large Eddy Simulations (*LES*). In *LES* one resolves the larger eddies and model the effects of the small (unresolved) scales on the resolved ones. The cut-off wave number is determined by the filter function. In this work the numerical scheme acts as a filter, with the filter size being proportional to the grid size. The dissipative effect of the smallest, unresolved, scales is handled by the inherent dissipation of the numerical scheme. This approach is adequate only when the spatial resolution is sufficient, *i.e.* when the energy cascade is independent of the numerical parameters (grid size and numerical scheme).

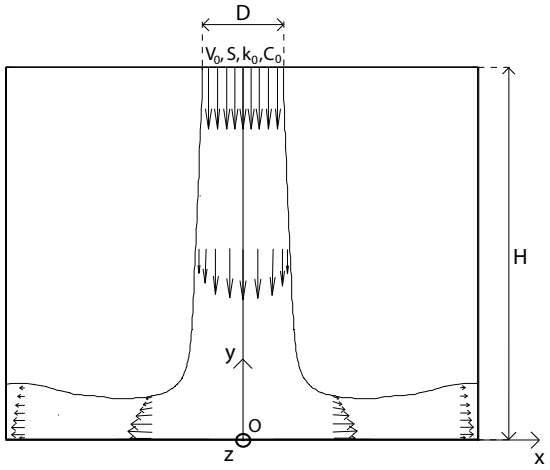

Figure 1. GEOMETRY OF IMPINGING JET (CROSS-SECTION).

The code is based on a staggered Cartesian grid and the discretization is performed by finite differences. To avoid masking of the Sub-Grid Scale (*SGS*) stress by the truncation error high order schemes are needed. The spatial discretization of the momentum equation uses a $O(h^4)$ central differences scheme for all terms except the advection term which is approximated by $O(h^3)$ upwind scheme, proposed by [8]. The discretization of the advection term adds enough dissipation to allow implicit *SGS* modeling, as verified by among others, [9] and [10]. Also, the influence of the small scales on the larger ones is accounted for. In this work no explicit *SGS* model has been used.

On average, the amount of (turbulent) energy in the small scales is independent of the numerical dissipation, provided that one can resolve a portion of the inertial sub-range. Thus, by having adequate resolution the numerical dissipation does not affect the large-scale results. If there is excessive numerical dissipation, a posteriori analysis of the turbulent energy spectrum would show the absence of the inertial sub-range. In the near wall region, the grid is highly resolved (using grid stretching). There are several grid nodes in the viscous sub-layer. For this reason, the no-slip condition is applied at the impingement wall, without any further attempt to add damping or using "wall functions". For the temporal discretization the time splitting scheme by [9] has been used.

PROBLEM SETUP

The impinging jet features a circular jet emanating from a nozzle into a large space limited by the impingement and the confinement wall. In Fig. 1 a cross-section of the impinging jet is shown. The confinement wall is located at the upper horizontal line, so also the nozzle outlet (*i.e.* velocity inlet). The impingement wall is located at the lower horizontal line, *i.e.* where

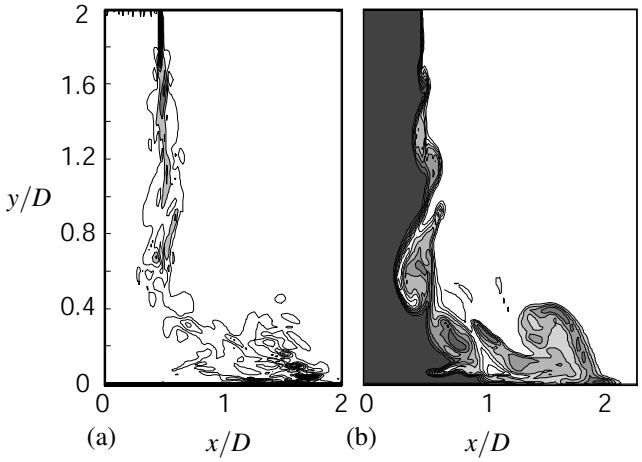

Figure 2. INSTANTANEOUS VORTICITY IN (a) AND INSTANTANEOUS CONCENTRATION IN (b).

$y/D = 0$. D, in the figure, is the diameter of the nozzle outlet, H is the height of the geometry and the letters with indices "0" are the characteristic parameters for the velocity- and the concentration fields at the nozzle outlet. The nozzle features a flat axial velocity profile, V_0, with superimposed random disturbances, k_0. The swirl-number, S, is defined as the azimuthal velocity, U_s, at $D/2$ divided by V_0. Solid body rotation is applied and the concentration as well as the velocities are set to zero at the walls. For normalization appropriate combinations of D, V_0 and C_0 are used.

As a complement to the comprehensive study of model behavior and grid dependency (for the present code) performed by [11] and [10], four different grids have been studied. These have $46*50*46$ (*grid1*), $194*98*194$ (*grid2*), $226*114*226$ (*grid3*) and $194*162*194$ (*grid4*) cells, respectively, on the finest out of five multi-grid levels. The average deviation between the three finer grids is a few percents why *grid2* is believed being a sufficient choice.

BASIC FEATURES OF IMPINGING JET FLOW

In the present configuration, the nozzle outlet velocity profile is, as known, flat. But as the jet leaves the nozzle, the influence from the surrounding, stagnant, fluid results in a strong axial shear layer. Figure 2(a) depicts the instantaneous vorticity in the *xy*-plane. As can be seen, the vorticity is intense close to the nozzle outlet and, hence, there are strong velocity gradients. The axial shear layer, which is axi-symmetric, is inherently unstable and initially symmetrical disturbances grow. These disturbances correspond to the, linear instability theory of a two-dimensional shear-layer (*i.e.* Kelvin Helmholtz instability), and implies that disturbances grow exponentially in the downstream direction.

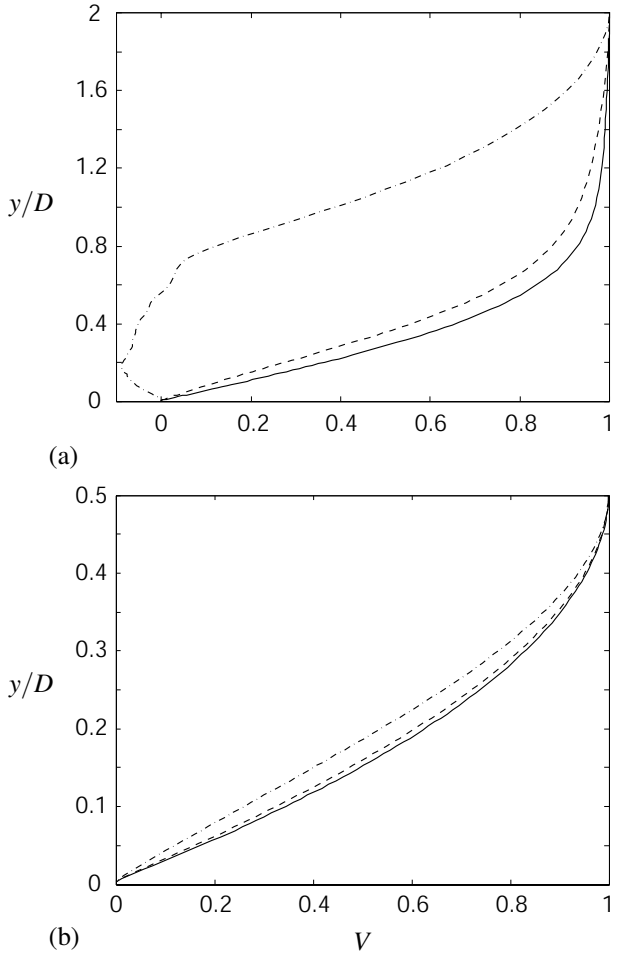

Figure 3. MEAN AXIAL VELOCITY DECAY ALONG THE STAGNATION LINE ($x/D = 0$) FOR $H/D = 2$ IN (a) AND $H/D = 0.5$ IN (b). (—): $S = 0$, (- - -): $S = 0.5$, (- · -): $S = 1$.

Slightly downstream from the nozzle, non-linear effects become significant and the linear approximation breaks down. Even further downstream there is a process featuring merging of vortices, that results in strong, so called, primary vortices, and halving of the characteristic frequency. The downstream development of the axial jet depends strongly on the inlet boundary conditions and on the shape of the nozzle, as shown in work by [1].

The primary vortices are deflected by the wall and convected in the wall parallel (radial) direction. Figure 2(b) clearly depicts, by means of instantaneous scalar concentration, the vortical motion. Depending on the strength and wall normal distance, these vortices may initiate formation of counter rotating, so called, secondary vortices. The motion of these vortices is the main reason for local flow separation (often referred to as turbulent separation). Additional to the, single frequency, large scale vortices

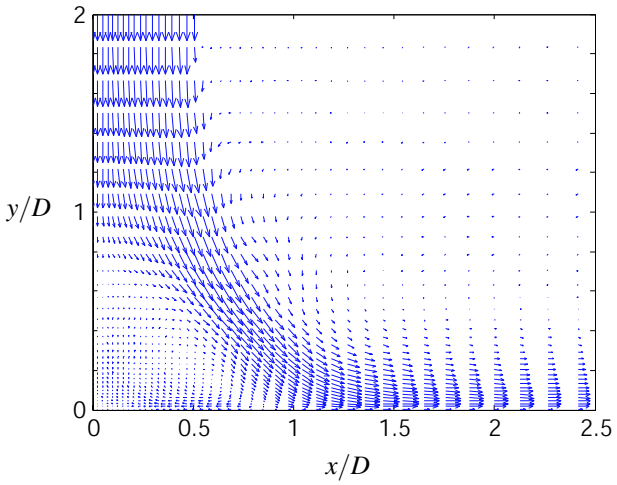

Figure 4. VELOCITY VECTORS IN THE xy-PLANE FOR $S = 1$. $H/D = 2$.

there are a wide range of chaotic structures, so called eddies. These structures defines the true level of turbulence (fulfilling the Kolmogorov's energy spectrum). The level of fluctuating velocity is given by the turbulent kinetic energy, k. There have been no attempts to divide the total energy into energy due to turbulence and energy due to periodical structures.

INFLUENCE FROM SWIRL

Two swirl rates, S, have been considered (S is either 0.5 or 1, respectively). Unfortunately, there are no experimental data available for comparison. The reason for this shortage is simply due to the fact that such experiments are very demanding. When using different swirl generators for small nozzle-to-plate spacings the impinging jet will not be circular anymore. Instead, the character becomes that of a segmented jet. This cause, among other things, an increased level of turbulence within the axial jet, due to strong interaction between the individual jet segments. For comparison between non-swirling circular and multiple impinging jets see [5].

A direct consequence with superimposed swirl is that an additional force, the centrifugal force, influences the flow field. This force is proportional to the inverse of the radial distance and to the square of the swirl velocity, U_s. The nozzle-to-plate spacing has strong influence on the development of the axial jet as swirl is applied, as seen in Figs. 3. Considering $H/D = 2$, Fig. 3(a), the mean axial velocity decay for case $S = 0.5$ is similar to the results for case $S = 0$. But as U_s is doubled ($S = 1$) the centrifugal force becomes four times as strong. This cause the spreading rate of the axial jet to increase, as the fluid is, basically, pushed out in the radial direction. At approximately $y/D = 0.5$

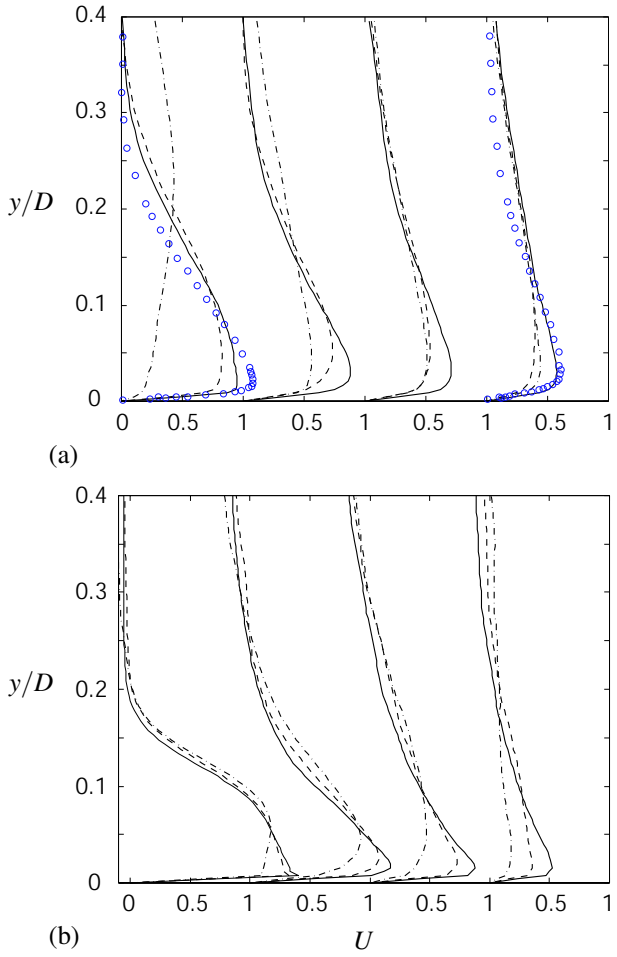

Figure 5. WALL PARALLEL DEVELOPMENT OF U FOR $H/D = 2$ IN (a) AND $H/D = 0.5$ IN (b). THE PROFILES ARE STAGGERED ACCORDING TO THEIR LONGITUDINAL LOCATION, $x/D = 1$, $x/D = 1.5$, $x/D = 2$ AND $x/D = 2.5$. (—): $S = 0$, (- - -): $S = 0.5$, (- · -): $S = 1$, (○): EXPERIMENTAL DATA BY [12] (Re=23000, $S = 0$).

the axial velocity becomes negative and a recirculation bubble is formed. However, in the cases of $H/D = 0.5$, Fig. 3(b), the results are similar for all three simulations. The spreading of the axial jet is only slightly affected by swirl. This is due to, overall, strong influence by the wall and, hence, lack of free jet behavior.

Figure 4 depicts the (increased) spreading rate of the axial jet for case $S = 1$, $H/D = 2$. The character of the axial flow, with the formation of a recirculation bubble in the center region, reminds of the vortex breakdown process for swirling free-jets, as described by, among others, [7]. In the case of vortex breakdown a recirculation region is formed, that acts as an obstacle that the fluid has to pass around. In three-dimensions the recirculation bubble seen in the stagnation region of the xy-plane corresponds

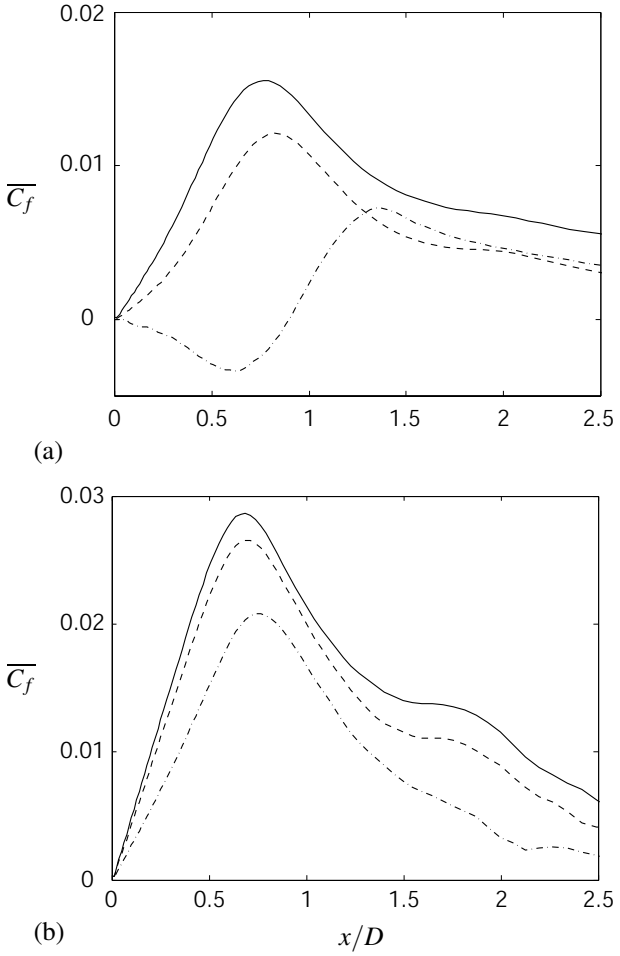

Figure 6. MEAN FRICTION COEFFICIENT, $\overline{C_f}$, FOR $H/D = 2$ IN (a) AND $H/D = 0.5$ IN (b). (—): $S = 0$, (- - -): $S = 0.5$, (- · -): $S = 1$.

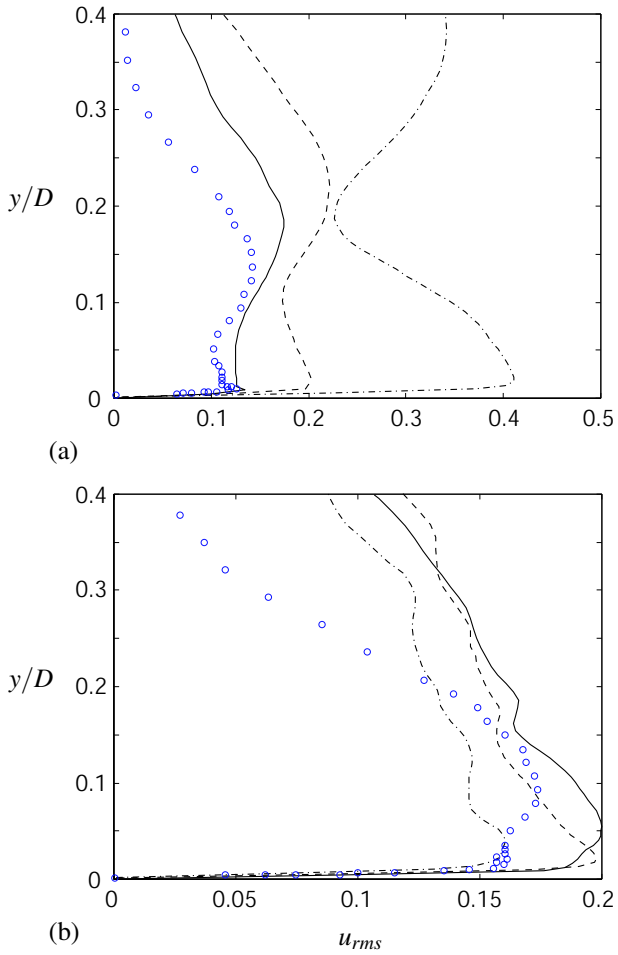

Figure 7. u_{rms} AT $x/D = 1$ IN (a) AND $x/D = 2.5$ IN (b). $H/D = 2$. (—): $S = 0$, (- - -): $S = 0.5$, (- · -): $S = 1$, (○): EXPERIMENTAL DATA BY [12] (Re=23000, $S = 0$).

to a rotating, donut shaped, structure.

The wall parallel development of U between $x/D = 1$ and $x/D = 2.5$ is depicted in Fig. 5(a) for the cases of $H/D = 2$. At $x/D = 1$ the strong spreading rate, in case of $S = 1$, is reflected in the smeared out velocity profile. Case $S = 0.5$ shows, as also observed above, only little deviation from the non-swirling flow. One step further downstream, at $x/D = 1.5$, the influence from swirl becomes strongly weakened and even further downstream all profiles collapse, at least in the outer region of the wall jet. The experimental results by [12] show good agreement with the non-swirling case. Particularly at $x/D = 2.5$ where the wall jet, only weakly, depends on the inflow conditions. For small nozzle-to-plate spacing, *i.e.* $H/D = 0.5$, the influence from swirl is weak for small x/D, as seen in Fig. 5(b). However, when going downstream the influence increases and the wall jet profiles show a tendency to become smeared out for increasing S.

The recirculation bubble obtained in case $S = 1$, $H/D = 2$ has a drastic influence on the near wall flow. As can be seen from the mean friction coefficient, $\overline{C_f}$, in Fig. 6(a) the flow attaches the wall as far downstream as $x/D = 1$. A direct consequence of this is that the Nusselt number in this region becomes largely reduced, as will be shown later. For $x/D > 1.4$ all three cases follow the same trend, but with slightly lower $\overline{C_f}$ for the two swirling cases. With smaller nozzle-to-plate spacing, Fig. 6(b), $\overline{C_f}$ show similar trend for all cases. However, as reflected in the profiles of U above, there is a monotone decrease of wall friction as S increases. The curves for case $S = 0.5$ and $S = 1$ do not collapse when going downstream, as they did for $H/D = 2$ in Fig. 6(a).

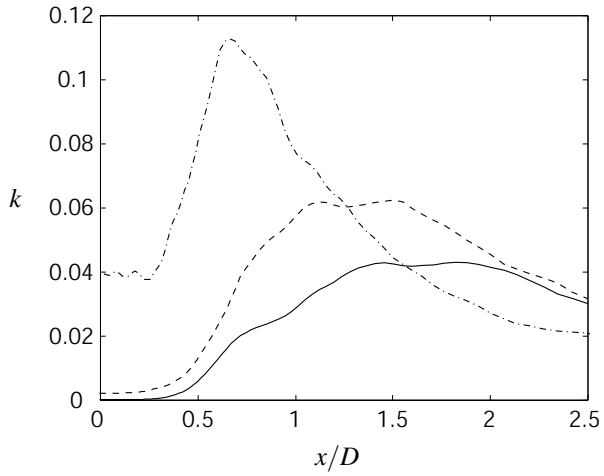

Figure 8. WALL PARALLEL DEVELOPMENT OF THE TURBULENT KINETIC ENERGY, k, AT $y/D = 0.15$. $H/D = 2$. (—): $S = 0$, (- - -): $S = 0.5$, (- · -): $S = 1$.

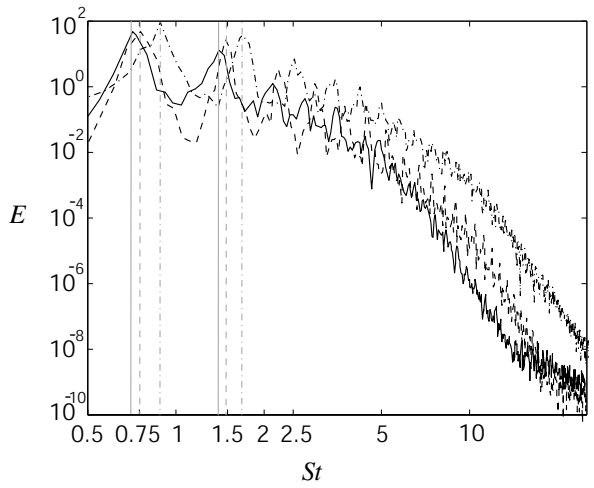

Figure 9. FREQUENCY SPECTRUM FOR u' AT $x/D = 0.5$, $y/D = 1$. $H/D = 2$. (—): $S = 0$, (- - -): $S = 0.5$, (- · -): $S = 1$.

TURBULENCE CHARACTERISTICS

For swirling impinging jets the turbulence production, in the axial jet, becomes augmented. This is so since there are strong mean flow gradients in the periphery of the axial jet, caused by shear between the azimuthal movement and the ambient non-swirling fluid. Initially this shear layer contains gradients of same order of magnitude as the, from axial momentum, initiated one. Figure 7(a) shows u_{rms} for the cases of $H/D = 2$ at $x/D = 1$. The results for case $S = 0$ and $S = 0.5$ are of same character, but with higher level of u_{rms} for the latter one. The location of the

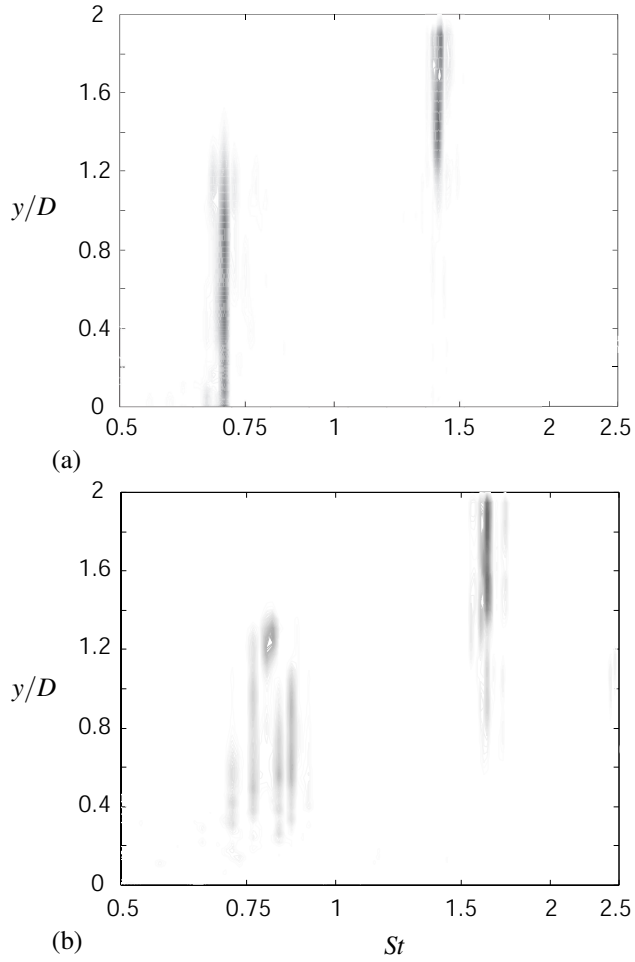

Figure 10. SPACE-FREQUENCY MAP ALONG $x/D = 0.5$ FOR u'. $S = 0$ IN (a) AND $S = 1$ IN (b). $H/D = 2$.

maximum value, in case of $S = 0.5$, is further away from the wall. This is coupled to the shape of the wall jet. For case $S = 1$ the re-circulation results in large values of u_{rms}. The high value close to the wall is due to the re-attachment point moving back and forth along the wall, making the local instantaneous radial velocity to shift abruptly between large positive and large negative values. The primary vortices are the main source of this oscillation. The experimental results by [12] show similar magnitude of u_{rms} in the near wall region as compared to the non-swirling simulation. The level in the outer region is lower, however the shape of the two profiles are of similar character.

Further downstream at $x/D = 2.5$, Fig. 7(b), case $S = 1$ show slightly lower value of u_{rms}, however, the trend is the same as for the other two. The results for case $S = 0$ and $S = 0.5$ are close to collapse. Hence, when going downstream the natural development of the wall jet cause the influence from the inlet conditions

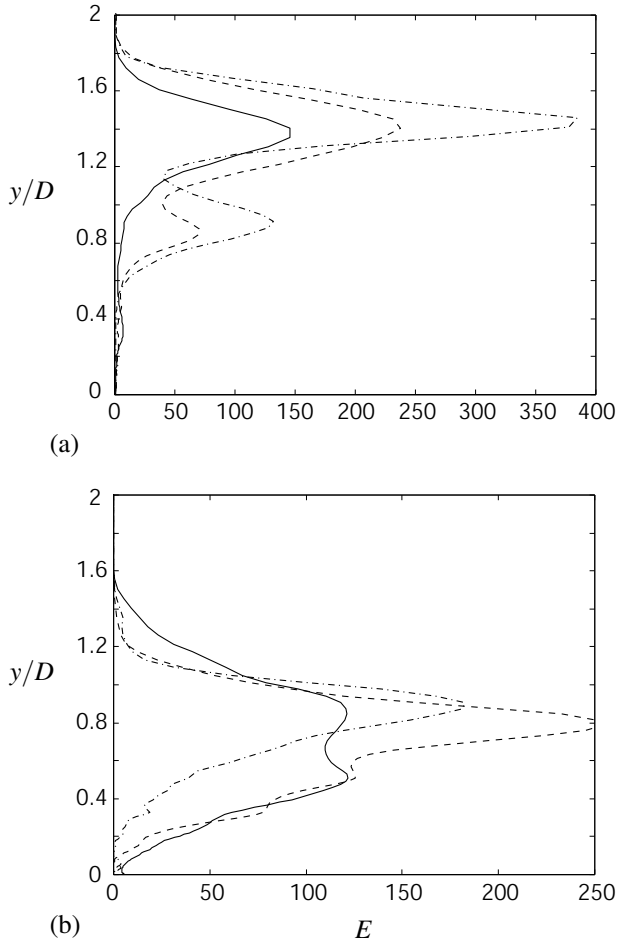

Figure 11. ENERGY LEVELS FOR St_f IN (a) AND St_{PV} IN (b), ALONG $x/D = 0.5$. $H/D = 2$. (—): $S = 0$ (St_f=1.4, St_{PV}=0.7), (- - -): $S = 0.5$ (St_f=1.5, St_{PV}=0.75), (- · -): $S = 1$ (St_f=1.64, St_{PV}=0.82).

to weaken, *i.e.* not only regarding S, but also for the level of k_0 and the shape of the inlet velocity profile, V_0. In the near wall region, the experimental and computational results show similar behavior. The downstream trend, featuring weakening of the inflow conditions, is also depicted in Fig. 8. This figure shows the wall parallel development of the turbulent kinetic energy, k, at $y/D = 0.15$. The results for case $S = 0$ and $S = 0.5$ are the same for $x/D > 2$ and the trend for case $S = 0.5$ and $S = 1$ is the same for $x/D > 1.5$. Close to the stagnation point only case $S = 1$ show significant levels of k, equalling 0.04. The high level for case $S = 1$ between $x/D = 0.5$ and $x/D = 1$ is, as mentioned before, due to the oscillation of the re-attachment point.

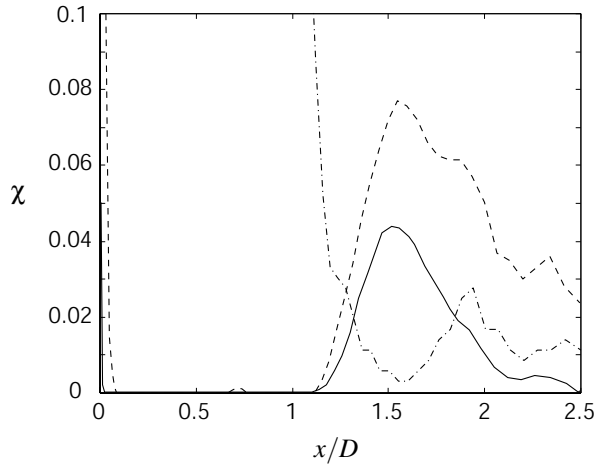

Figure 12. BACK-FLOW COEFFICIENT , χ, IN THE VICINITY OF THE WALL FOR $H/D = 2$. (—): $S = 0$, (- - -): $S = 0.5$, (- · -): $S = 1$.

STRUCTURES AND DYNAMICS

Non-swirling flow features, in the current configuration of $H/D = 2$, distinct formation of periodical structures. The fundamental frequency, St_f, corresponding to the axi-symmetric vortex roll-up in the vicinity of the nozzle outlet, is equal to 1.4. In the vortex pairing process, primary vortices are alternatingly shed with a frequency, St_{PV}, equal to 0.7, *i.e.* a sub-harmonic frequency. As swirl is applied these frequencies become higher. Figure 9 depicts the frequency spectrum for u' within the axial shear layer at $x/D = 0.5$, $y/D = 1$. The fundamental frequency for case $S = 0.5$ and $S = 1$ is found to be 1.5 and 1.64, respectively. The sub-harmonics are 0.75 and 0.82, respectively. It should be emphasized that with increasing swirl, the sub-harmonic, and, to some extent, also the fundamental frequency become less distinct (*i.e.* there are several of them in a near range). This is the result of the interaction of the azimuthal mode instability (due to azimuthal shear) with the base flow instabilities (due to axial shear). These features are possible to identify in Figs. 10, which show the space-frequency map for u' in the axial shear layer. Figure 10(a) shows the characteristic behavior for case $S = 0$ and Fig. 10(b) for case $S = 1$. Note that in the latter figure, the spreading of the axial jet also influences the spectrum, *i.e.* for small y/D. Except from the broaden spectrum, the figures clearly show the vortex pairing process, as the characteristic frequency jumps from St_f to St_{PV}.

In Fig. 9 the energy content of the two characteristic frequencies seemed to be higher for increased level of swirl. To sort this out, Figs. 11 depict the downstream development of structures featuring St_f and St_{PV} in the axial shear layer. As shown in Fig. 11(a) the growth rate of St_f is overall strongest for case $S = 1$ as going downstream from the nozzle outlet at $y/D = 2$. Hence,

the azimuthal velocity contributes to (”triggers”) the formation of, not only chaotic, but also periodical structures. Initially, the two swirl cases show same growth of St_f, whereas for case $S = 0$ it is substantially lower. The two cases featuring $S > 0$, shows a second maximum located, approximately, at $y/D = 0.85$. The existence of these peaks may be attributed to energy exchange between structures with adjacent frequencies (broaden spectrum), however, the mechanism behind these interactions is unclear and requires further investigation. These two maximums are located at almost identical y/D-value, as for the two maximums of St_{PV} in Fig. 11(b). The growth of St_{PV} is, in contradiction to the behavior just mentioned, initially strongest for case $S = 0$. However, further downstream the swirling cases dominate. In case $S = 1$ the large spreading of the jet may be a reason to the lower energy level of St_{PV}, as compared to that of case $S = 0.5$. The same mechanism may also explain the monotone reduction of energy (to zero) being initiated further upstream. This is so since the vortical structures are most energetic in the shear layer and not within the core region of the axial jet.

The probability for separation can be defined by the back-flow coefficient χ, defined as

$$\chi(x,y) = \frac{1}{N}\sum_{k=1}^{N}\left(1 - sgn(u^k(x,y))\right), \qquad (3)$$

where u is the instantaneous velocity in the xy-plane at $z = 0$, N is the total number of samples and sgn is the sign-function. χ as function of x/D is shown in Fig. 12 for case $S = 0$, $S = 0.5$ and $S = 1$. The peak level of χ for $S = 0.5$ is 3 percents higher compared to non-swirling flow, however the maximum occurs at the same location. The high energy level of St_{PV}, seen in Fig. 11(b) (case $S = 0.5$), is probably of great importance for the increase of χ, as strong secondary vortices are more capable to initiate counter rotating secondary vortices. Due to the formation of a recirculation bubble for case $S = 1$, the character of the wall jet changes. The high levels of χ for $x/D < 1.5$ is, of course, due to back-flow. As the flow re-attaches, the probability for separation becomes lower compared to the two other cases.

HEAT TRANSFER

The influence of swirl on the scalar transport is briefly discussed in this section. The main purpose is to obtain a qualitative understanding of the mixing of scalars in the presence of swirl. Figures 13 depict the downstream development of the mean concentration, C, in the wall jet for case $S = 0$, $S = 0.5$ and $S = 1$. In Fig. 13(a), showing $H/D = 2$, there seem to be a monotone dependence of the swirl number, as the profiles for C become successively steeper for increasing S. This is most obvious for small x/D. For the U-velocity in Fig. 5(a), this kind of behavior where only seen for case $S = 0$ and $S = 0.5$. In the strongest

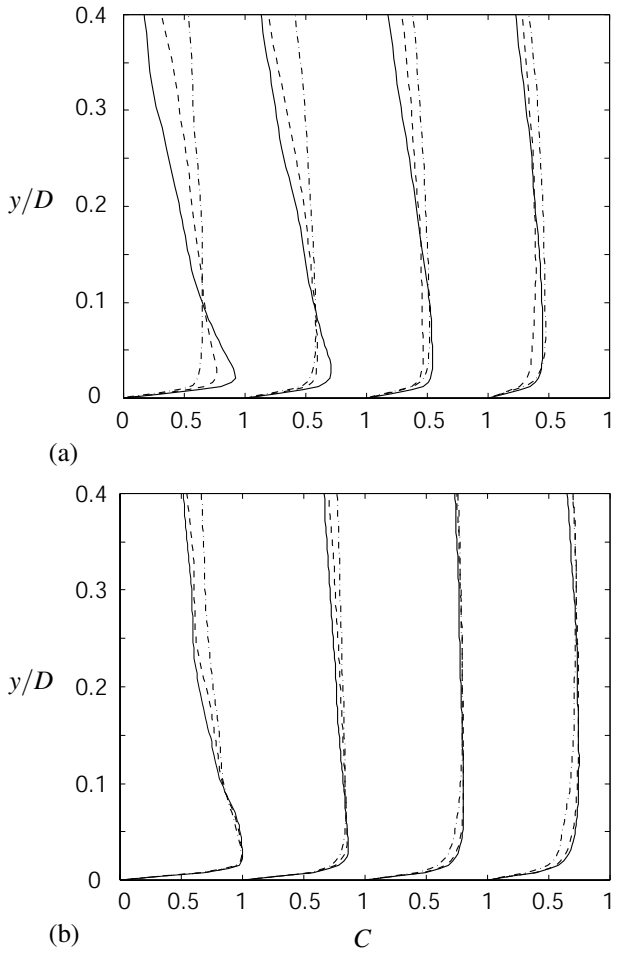

Figure 13. WALL PARALLEL DEVELOPMENT OF C FOR $H/D = 2$ IN (a) AND $H/D = 0.5$ IN (b). THE PROFILES ARE STAGGERED ACCORDING TO THEIR LONGITUDINAL LOCATION, $x/D = 1$, $x/D = 1.5$, $x/D = 2$ AND $x/D = 2.5$. (—): $S = 0$, (- - -): $S = 0.5$, (- · -): $S = 1$.

swirling case, the wall jet was heavily widen, due to the formation of a recirculation bubble. However, the development of the scalar is influenced by all three velocity components and, hence, the differences between U and C are not that surprising. For the cases of $H/D = 0.5$, shown in Fig. 13(b), swirl has no significant influence on the scalar field.

The distribution of turbulent scalar flux, $\overline{u'c'}$, is depicted in Figs. 14. Fig. 14(a) shows the distribution at $x/D = 1$ and Fig. 14(b) at $x/D = 2.5$. $\overline{u'c'}$ is the dominant flux term in the xy-plane, in the same way $\overline{w'c'}$ is the dominant flux term in the yz-plane. At $x/D = 1$, case $S = 0$ and $S = 0.5$ show similar behavior, whereas $\overline{u'c'}$ for case $S = 1$ is much stronger in the wall adjacent and outer shear layers. This is coupled to the character

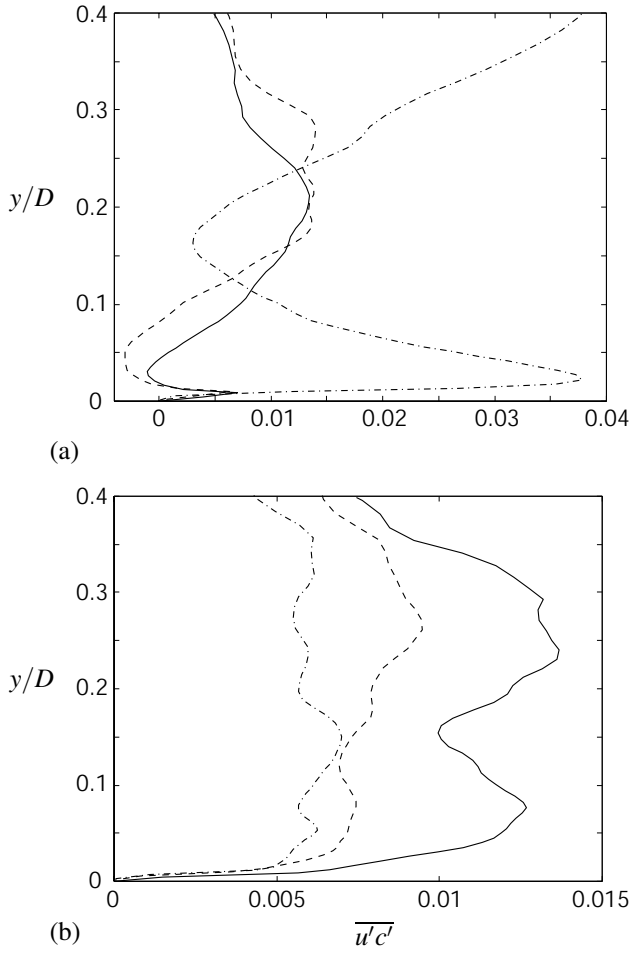

Figure 14. SCALAR FLUX, $\overline{u'c'}$, AT $x/D = 1$ IN (a) AND $x/D = 2.5$ IN (b). $H/D = 2$. (—): $S = 0$, (- - -): $S = 0.5$, (- · -): $S = 1$.

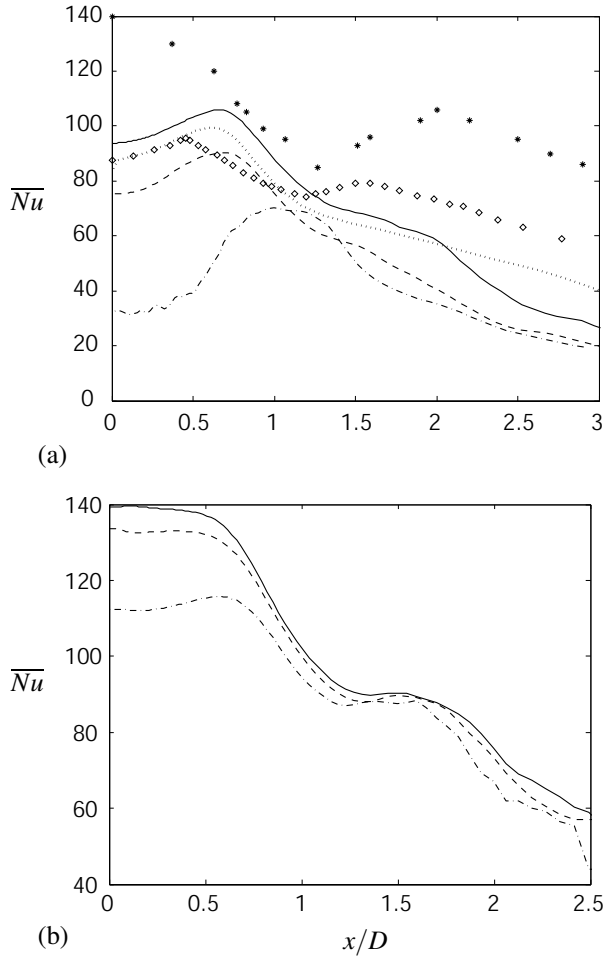

Figure 15. MEAN NUSSELT NUMBER FOR $H/D = 2$ IN (a) AND $H/D = 0.5$ IN (b). (—): $S = 0$, (- - -): $S = 0.5$, (- · -): $S = 1$, (· · ·): RNG $k-\varepsilon$ ([13], Re=20000, $S = 0$), (∗): [14] (Re=23000, $S = 0$), (◇): [15] (Re=10000, $S = 0$).

of u_{rms} in Fig. 7(a). Further downstream, at $x/D = 2.5$, the turbulent flux for case $S = 0$ show similar behavior as the u_{rms}. For the swirling cases $\overline{u'c'}$ becomes weaker.

The mean Nusselt number, $\overline{Nu}$, as function of x/D is depicted in Figs. 15. The first peak in Fig. 15(a) is commonly attributed to a local thinning of the velocity boundary layer, as the velocity of the wall jet is locally high. The second peak, which is clearly visible in the experimental data, is commonly claimed to be due to induced interacting vortices (secondary vortices) between the large-scale vortices (primary vortices) and the impingement wall and by transition from a laminar to a turbulent wall jet. This has been studied by, among others, [16]. The difference between the numerical and experimental results for case $S = 0$, is partly due to the difference in inflow boundary conditions. Except from the level of fluctuations, the shape of the mean velocity profile at the nozzle outlet is also of great importance ([3]). Equally important is the geometrical shape of the nozzle outlet ([17]). The experiments featured, in contradiction to the *LES* simulation, fully developed pipe flow. The above discussed vortical structures can not be captured by the RANS based RNG $k-\varepsilon$ model. This is one reason why there is no second maximum of $\overline{Nu}$.

As was seen in Fig. 6(a), the recirculation region reached as far downstream as $x/D = 1$ for case $S = 1$. A direct consequence of this is that the mean Nusselt number in this region becomes highly obstructed. This is depicted in Fig. 15(a). Consequently, when swirl is applied there is a region, approximately limited to the stagnation region, $|x/D = 1.25|$, in which the overall heat transfer decreases. Downstream of this region the influence from swirl decreases. The decrease in Nusselt number with increased

level of swirl is also documented in the work by [5]. This matter is of great importance as in many practical applications swirling flows are used. For instance in fan-cooling applications. To solve this problem the level of turbulence needs to be increased, in an attempt to balance the losses caused by the jet spreading. However, if the nozzle-to-plate spacing is large, such that, the axial jet is fully developed (approximately larger than $H/D = 7$, as shown in the work by [2]), the high turbulence level may have an obstructing effect. The reason for this is the significant level of entrainment of, low momentum, ambient fluid.

With a nozzle-to-plate spacing equal to 0.5 no recirculation bubble (vortex breakdown) is present, and the Nusselt number is only slightly influenced by swirl, as depicted in Fig. 15(b). Due to the same phenomenon as discussed above, the stagnation Nusselt number decreases for increasing swirl. The second peak of $\overline{Nu}$ seems to move in the upstream (proximal) direction as S increases. This may be attributed to the increasing level of turbulence in the axial jet, which, as shown before, promotes the development of the wall jet.

CONCLUSIONS

Basic studies of the dynamics and character of the circular impinging jet have been carried out, both for non-swirling and swirling flows and for different nozzle-to-plate spacings. The benefits using *LES* instead of *RANS*-based methods are revealed from studies of time-series, correlations and spectrums. The *LES* studies have been useful for understanding the transition process and the relation between the flow- and scalar fields. Some phenomena that have been captured include the formation of primary- and counter-rotating secondary vortices and vortex breakdown at higher swirl numbers. Separation due to strong secondary vortices have also been captured. Dominant frequencies and correlations between the flow- and scalar-fields have been studied in some detail.

The results show that swirl has a negative effect on heat-transfer in the stagnation region. This is so even though the energy of the velocity fluctuations is higher as compared to the non-swirling case. Convective transport is thus of great importance in this region. For small nozzle-to-plate spacings, the influence of swirl is not highly pronounced, as the axial jet does not experience the same degree of spreading. However, swirl enhances mixing and with high enough swirl, the presence of vortex breakdown leads to a larger stagnation region at the impingement wall. To achieve efficient impingement cooling the swirl level of the axial jet should be kept as low as possible. In the case of fan applications guide vanes can be used to dampen the azimuthal velocity component.

ACKNOWLEDGMENT

The author wish to thank his supervisor Prof. Laszlo Fuchs for sharing his thoughts and knowledge and also his employer and financier Scania CV AB for making all this possible.

REFERENCES

[1] Liu, T., and Sullivan, J. P., 1996. "Heat transfer and flow structures in an excited circular impinging jet". *Int. J. Heat Mass Transfer,* **39** , pp. 3695–3706.

[2] Hwang, S., Lee, C., and Cho, H., 2001. "Heat transfer and flow structures in axisymmetric impinging jet controlled by vortex pairing". *Int. J. Heat and Fluid Flow,* **22** , pp. 293–300.

[3] Behnia, M., Parneix, S., Shabany, Y., and Durbin, P., 1999. "Numerical study of turbulent heat transfer in confined and unconfined impinging jets". *Int. J. Heat and Fluid Flow,* **20** , pp. 1–9.

[4] Huang, L., and El-Genk, M., 1998. "Heat transfer and flow visualization experiments of swirling, multi-channel, and conventional impinging jets". *Int. J. Heat Mass Transfer,* **41** , pp. 583–600.

[5] Lee, D. H., Won, S. Y., Kim, Y. T., and Chung, Y. S., 2002. "Turbulent heat transfer from a flat surface to a swirling round impinging jet". *Int. J. Heat Mass Transfer,* **45** , pp. 223–227.

[6] Sarpkaya, T., 1971. "On stationary and traveling vortex breakdowns". *J. Fluid. Mech.,* **45** , pp. 545–559.

[7] Billant, P., Chomaz, J.-M., and Huerre, P., 1998. "Experimental study of vortex breakdown in swirling jets". *J. Fluid Mech.,* **376** , pp. 183–219.

[8] Rai, M. M., and Moin, P., 1991. "Direct simulation of turbulent flow using finite difference schemes". *J. Comput. Phys.,* **96** , pp. 15–35.

[9] Olsson, M., and Fuchs, L., 1998. "Large eddy simulation of a forced semi-confined circular impinging jet". *Phys. Fluids,* **10** , pp. 476–486.

[10] Revstedt, J., 1999. *On the modeling of Turbulent Flow and Mixing in Stirred Reactors*. PhD Thesis, Division of Heat Transfer, Department of Heat and Power Engineering, Lund Institute of Technology, Lund.

[11] Olsson, M., 1997. *Large Eddy Simulation of Turbulent Jets*. PhD Thesis, Dept. Mechanics, Royal Institute of Technology, Stockholm, January.

[12] Cooper, D., Jackson, D., Launder, B., and Liao, G., 1993. "Impinging jet studies for turbulence model assessment-i. flow field experiments". *Int. J. Heat and Fluid Flow,* **36** , pp. 2675–2684.

[13] Hallqvist, T., 2003. *Numerical study of impinging jets with heat transfer*. Licentiate thesis, Dept. Mechanics, Royal Institute of Technology, Stockholm, May.

[14] Yan, X., and Saniei, N., 1997. "Heat transfer from an

obliquely impinging circular jet to a flat plate". *Int. J. Heat and Fluid Flow,* **18** , pp. 591–599.

[15] Lee, D. H., Lee, Y. M., Kim, Y. T., Won, S. Y., and Chung, Y. S., 2002. "Heat transfer enhancement by the perforated plate installed between an impinging jet and the target plate". *Int. J. Heat Mass Transfer,* **45** , pp. 213–217.

[16] Lee, J., and Lee, S.-J., 2000. "The effect of nozzle aspect ratio on stagnation region heat transfer characteristics of elliptic impingement jet". *Int. J. Heat Mass Transfer,* **43** , pp. 555–575.

[17] Lee, J., and Lee, S.-J., 2000. "The effect of nozzle configuration on stagnation region heat transfer enhancement of axisymmetric jet impingement". *Int. J. Heat Mass Transfer,* **43** , pp. 3497–3509.